

## Article

# Temperature Prediction of Icy Lunar Soil Sampling Based on the Discrete Element Method

Deming Zhao <sup>1</sup>, Tianyi Peng <sup>1</sup>, Weiwei Zhang <sup>2,\*</sup>, He Wang <sup>1</sup> and Jinsheng Cui <sup>3</sup>

<sup>1</sup> School of Mechanical Engineering, Zhejiang Sci-Tech University, Hangzhou 310018, China; zdm@zstu.edu.cn (D.Z.); 2023220503114@mails.zstu.edu.cn (T.P.); 202030605254@mails.zstu.edu.cn (H.W.)

<sup>2</sup> State Key Laboratory of Robotics and System, Harbin Institute of Technology, Harbin 150001, China

<sup>3</sup> School of Mechanical and Electrical Engineering, Guangzhou University, Guangzhou 510006, China; meecuijs@gzhu.edu.cn

\* Correspondence: zweier@hit.edu.cn

**Abstract:** This study is part of the preliminary research for the Chang'e 7 project in China. The Chang'e 7 project plans to drill to penetrate the lunar polar soil and collect lunar soil samples using a spiral groove structure. Ice in the cold environment of the lunar polar region is one of the important targets for sampling. In the vacuum environment of the lunar surface, icy soil samples are sensitive to ambient temperature and prone to solid–gas phase change as the temperature increases. To predict the temperature range of lunar soil samples, this study analyzed the effect of thermal parameters on the temperature rise of lunar soil particles and the drill using discrete element simulation. The parameters included in the thermal effect analysis included the thermal conductivity and specific heat capacity of the drilling tools and lunar soil particles. The simulation showed that the temperature of the icy lunar soil sample in the spiral groove ranged from  $-127.89$  to  $-160.16$  °C within the thermal parameter settings. The magnitude of the value was negatively correlated with the thermal conductivity and specific heat capacity of the lunar soil particles, and it was positively correlated with those of the drilling tools. The temperature variation in the drill bit ranged from  $-51.21$  to  $-132$  °C. The magnitude of the value was positively correlated with the thermal conductivity and specific heat capacity of the lunar soil particles and the thermal conductivity of the drilling tool.

**Keywords:** lunar exploration; icy lunar soil; discrete element method; temperature prediction



**Citation:** Zhao, D.; Peng, T.; Zhang, W.; Wang, H.; Cui, J. Temperature Prediction of Icy Lunar Soil Sampling Based on the Discrete Element Method. *Aerospace* **2024**, *11*, 400. <https://doi.org/10.3390/aerospace11050400>

Academic Editor: Paolo Tortora

Received: 28 March 2024

Revised: 11 May 2024

Accepted: 13 May 2024

Published: 16 May 2024



**Copyright:** © 2024 by the authors. Licensee MDPI, Basel, Switzerland. This article is an open access article distributed under the terms and conditions of the Creative Commons Attribution (CC BY) license (<https://creativecommons.org/licenses/by/4.0/>).

## 1. Introduction

The formation and evolution of water on the lunar surface are one of the scientific objectives of national lunar exploration programs [1–3]. Studies [4–6] show that water exists in the form of fine crystals in permanently shadowed craters at the lunar poles. Ref. [7] report the detection of infrared signals from water molecules in the unshaded region of the lunar surface, confirming the existence of molecular water on the surface. The Diviner payload carried by the Lunar Reconnaissance Orbiter (LRO) carried out an internal exploration of the permanently shadowed area at the bottom of the crater in the polar region of the Moon and analyzed the possible areas of surface water ice and water-ice-bearing lunar permafrost through the results of the surface and subsurface temperature characteristics of the Moon's south pole, which were obtained from the LCROSS observations and the model calculations. Their endowment may be in the form of a mixture of ice and lunar soil or as water ice or bound water. The fact that water may be present in many forms means that the target of sampling operations in the polar regions will not be limited to anhydrous bulk lunar soil or lunar rocks but may also include a variety of material forms, such as ice–soil mixtures, water-absorbing rocks, and pure ice [8,9]. Water undergoes a solid–gas phase change at about  $-70$  to  $-60$  °C under vacuum, according to its phase change properties [10]. Accurate knowledge of soil temperature during drilling is the key to developing and optimizing a drilling sampling program. Currently, it is very difficult

and expensive to obtain a sample temperature in a low-temperature, high-vacuum test environment. In this study, to resolve the conflict between cost, ambiguity of thermal parameters, and importance of temperature information, a simulation method was used to predict the correlation between machine soil thermal parameters and drilling system temperature within a range of parameters.

Currently, the study of lunar drilling by discrete element method (DEM) mainly focuses on the force load on the drilling tool, the influence of bit configuration on the load, and the optimization of chip removal from the drilling tool [11]. A few researchers have investigated the thermal properties of lunar drilling using DEM numerical simulation techniques. Ref. [12] investigated the thermodynamic problems of drilling bits using the DEM method. Their results showed that the temperature rise in the simulated lunar soil in a vacuum environment was lower than the temperature rise of drilling under normal pressure. Ref. [13] introduced a particle contact heat transfer model into the DEM and analyzed particle heat transfer.

Previous research has confirmed the validity of the DEM for heat transfer studies in particulate systems. In this study, lunar soil samples were collected using a spiral trough structure, and discrete element modeling of icy lunar soil was performed. The model was based on the heat transfer model for lunar soil drilling proposed by [14]. In the simulation of the drilling process, the average temperature measurement area was the deep spiral groove area of 21 mm in diameter and 30 mm in height behind the drill bit. The Central Composite Design (CCD) method was used to derive the influence patterns of various thermodynamic parameters on the average lunar soil temperature and drill bit temperature. The results show that it is possible to predict lunar soil temperatures in deep spiral troughs when sample temperatures are difficult to obtain by experimental methods.

## 2. Simulation Model

### 2.1. Design for Sampling

Domestic and international research on lunar soil sampling equipment is mainly divided into two categories: manual sampling and drilling sampling. The Chang'e 7 project plans to use drilling to penetrate the polar lunar soil after the lander lands on the lunar surface. After the drilling tool reaches the target depth, it will stop feeding. After load stabilization, the drill will be lifted, and lunar soil samples will be extracted from the spiral groove structure. The sampling process is shown in Figure 1.

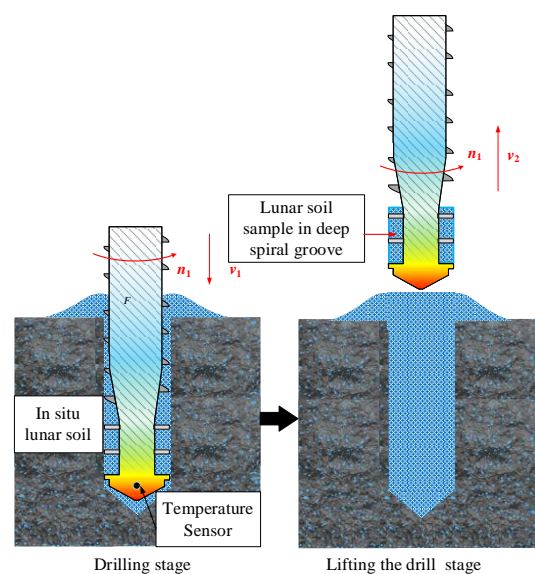


**Figure 1.** The sampling process.

The temperature measurement area is the average temperature of the lunar soil in the deep spiral groove and the drill bit at different moments. The temperature measurement point of the experimental bit and the simulation temperature measurement area are shown in Figure 2.

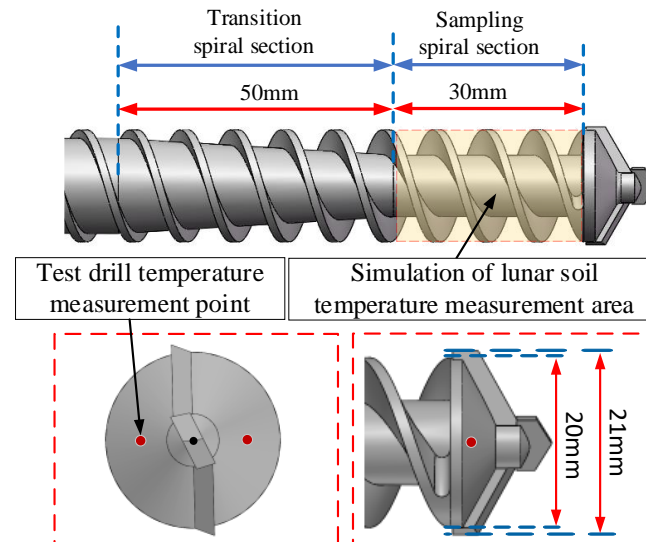


**Figure 2.** Temperature measurement point and temperature measurement area.

## 2.2. DEM Simulation Model and Test Equipment

The DEM simulation model included the machine and particle system components. Drill bits, drill pipes, and other tools were collectively referred to as geometry. In DEM simulation, the number of particles is one of the most important factors affecting the model size and calculation time. When building a simulated lunar soil, too many particles will cause the simulation time to be too long. In order to reduce the number of particles and ensure a certain simulation accuracy, this study used a multi-level particle size simulation model, created elongated particles and angular particles, and mixed them in a 1:1 ratio so that the non-spherical simulated lunar soil particles could be used as the real simulated lunar soil [14,15]. The basic idea is to divide the simulated lunar soil into a number of regions; the first region is the region directly interacting with and near the drilling rig. The mobility of particles in this region is more obvious, so smaller particle diameters are used for modeling in this region. Then, the rest of the simulated lunar soil, from inside to outside, is divided into two to three regions. These regions of the simulation of the lunar soil play the role of boundary conditions; mobility is weak in these regions, and a larger particle diameter is used for modeling. The particle diameter of the peripheral region gradually increases based on the size of the first region, and the aim is to reduce the number of particles down to the minimum. This reduces the amount of computation and saves computational time without affecting the computational accuracy too much. Based on the multi-level particle size simulation model, a drilling simulation lunar soil bucket was constructed, as shown in Figure 3a. The outer diameter of the bucket was 10 mm larger than the drilling impact area. In this study, the drilling tool was divided into 30 elements in the axial direction, as shown in Figure 3b. The length of each micro-element was 5 mm, and each micro-element was assumed to have the same temperature.

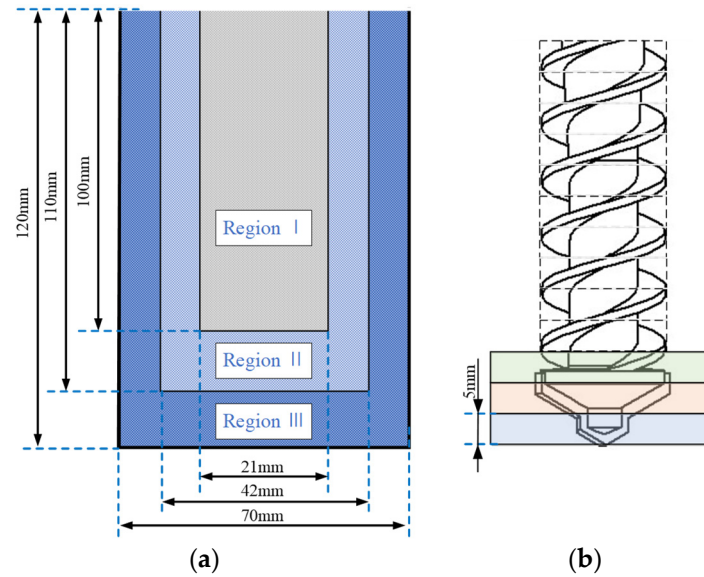


**Figure 3.** Lunar soil layer modeling and drilling tool microelement: (a) lunar soil layer modeling; (b) drilling tool microelement.

Heat transfer during lunar soil drilling consisted of two main components: (a) interparticle heat conduction, interparticle convection, and interparticle radiation; (b) heat conduction, convection, and thermal radiation between particles and geometry. Computational models for heat transfer between particles have been investigated in recent discrete element heat transfer studies. The heat transfer between particles  $i$  and  $j$  is given by the following equation [13]:

$$Q_{ij} = 2k_s(T_j - T_i) \left( \frac{3F_n r^*}{4E^*} \right)^{\frac{1}{3}} \quad (1)$$

where  $Q_{ij}$  is the heat transfer rate between particles;  $k_s$  is the thermal conductivity of granular materials;  $T_j$  and  $T_i$  are the temperatures of particles  $i$  and  $j$ ;  $F_n$  is the normal force between particles;  $E^*$  is the equivalent Young's modulus,  $E^* = \left( \frac{1-\nu_i^2}{E_i} - \frac{1-\nu_j^2}{E_j} \right)^{-1}$ ;  $r^*$  is the equivalent radius,  $r^* = \frac{r_i r_j}{r_i + r_j}$ , where  $r_i$  and  $r_j$  are the radius of particle  $i$  and  $j$ ;  $T_i$  and  $T_j$  are the temperature of particles  $i$  and  $j$  ( $^{\circ}\text{C}$ ).

The above model considers only heat conduction between particles, ignoring convective and radiative heat transfer. Other forms of heat transfer can be equated to the effective thermal conductivity of the particles. This simplifies the heat transfer model. According to the heat transfer relationship between two particles, if particle  $i$  is in contact with  $n$  particles, then the temperature change in particle  $i$  can be calculated according to the following equation:

$$\frac{dT_i}{dt} = \frac{\sum_{j=1}^n Q_{ij}}{\rho_i c_i V_i} \quad (2)$$

where  $t$  is the time (s);  $n$  is the number of particles in contact;  $\rho_i$  is the density of particle  $i$  ( $\text{kg}/\text{m}^3$ );  $c_i$  is the specific heat capacity of particle  $i$  ( $\text{J}/(\text{kg}\cdot^{\circ}\text{C})$ );  $V_i$  is the volume of particle  $i$  ( $\text{m}^3$ ).

The drilling experiment in a realistic environment is based on a 300 mm drilling test rig. The test rig is shown in Figure 4. The fixture provides a minimum ambient temperature of  $-196^{\circ}\text{C}$ . It ensures that the atmospheric environment of the drilling area is nitrogenous and is completely isolated from the external environment. This test fixture is used to obtain the temperature of the drill bit using a sensor in the drill bit. However, it is not possible to obtain the average temperature of the lunar soil in the deep spiral groove. In this study, the temperature of the sample area was predicted by simulation.

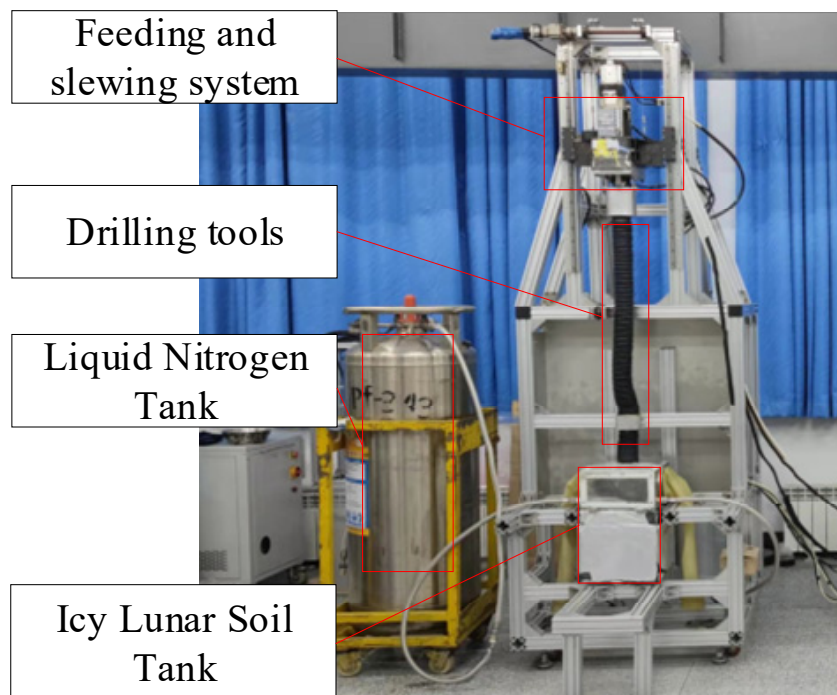


Figure 4. Experimental device.

### 2.3. Simulation Condition Settings and Thermal Simulation Verification

The experimental and simulation conditions were set, as shown in Table 1.

Table 1. Experimental settings and results.

Sample Moisture Content	Rotation Rate (r/min)	Feed Rate (mm/min <sup>-1</sup> )	Maximum Temperature Rise of the Drill Bit (°C)		Correlation Coefficient	Maximum Relative Error
			Experiment	Simulation		
5 wt%	250	63.29	65.50	72.35	0.9912	10.46%

Each thermal parameter used in the simulation is shown in Table 2.

Table 2. Thermal parameters of the simulation.

Parameter	Thermal Conductivity of Particles (W/(M·K))	Specific Heat Capacity of Particles (J/(kg·°C))	Thermal Conductivity of the Drill (W/(m·K))	Specific Heat Capacity of the Drill (J/(kg·°C))
	50.5	600	27.5	600

The effective thermal conductivity in the simulation was similar to the thermal conductivity of the actual icy lunar soil particles. Although the parameter fitting did not consider the actual physical significance of the effects of the parameters, it did fit the influence law at the numerical level for the range of simulation parameters. Therefore, some calibration parameters may be significantly different from those of the actual material. The comparison between simulation and experimental results is shown in Figure 5.

The results showed that the drill bit temperature curve of the simulation model was close to the trend of the actual test data curve when the moisture content was 5%. This confirmed the validity of the heat transfer model and the discrete element method. The maximum temperature difference between the two occurred at 150 s. The maximum temperature difference was 6.85 °C. The correlation coefficient *r* was greater than 0.99,

indicating a very high correlation between the actual and simulated data. Therefore, the simulation model can be used to predict the average temperature of the lunar soil in the deep spiral groove.

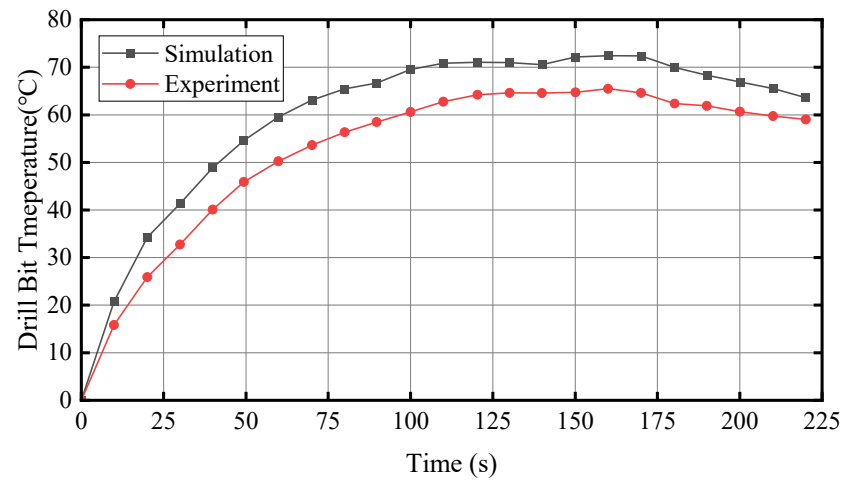


**Figure 5.** Experimental and simulation temperature variation graphs.

### 3. Temperature Prediction with Different Thermodynamic Parameters

#### 3.1. Simulation Parameter Classification and Impact Analysis

From Equations (1) and (2), the system includes parameters, as shown in Table 3. The parameters mainly include four categories, which are lunar soil drilling parameters, lunar soil heat transfer parameters, machine soil interaction parameters, and machine soil heat transfer parameters. Zhao et al. (2015) [16] performed a parameter-matching analysis on the lunar soil base parameters in a discrete element simulation and calibrated the lunar soil action parameters and machine soil action parameters. The DEM particle parameters were set as shown in Table 3, where the particle parameters were obtained by the calibration method of Deng et al. (2017) [17].

**Table 3.** The simulation parameters.

Parameter Number	Parameter Type	Parameter Items	Unit	Value/Range	Parameter Remarks
1	Lunar interaction parameters	Moisture content	wt %	5 (0–10)	Literature [18] and engineering environmental setting documentation
2		Lunar soil particle density	kg/m <sup>3</sup>	3000	Literature [19,20] and actual measurements, high certainty
3		Shear modulus	Pa	$3 \times 10^9$ ( $4 \times 10^7$ – $1 \times 10^{10}$ )	Literature [19,20] and simulation experience
4		Poisson's ratio	-	0.25 (0.2–0.3)	Basic material properties, high certainty
5		Static friction coefficient	-	0.8	Literature [16,20] and simulation experience
6		Rolling friction coefficient	-	0.6	Literature [16,20] and simulation experience
7		Coefficient of restitution	-	0.25	Literature [16,20] and simulation experience

Table 3. Cont.

Parameter Number	Parameter Type	Parameter Items	Unit	Value/Range	Parameter Remarks
8	Heat transfer parameters of lunar soil	Thermal conductivity of particles	W/(m·K)	50.5 (1–100)	Parameter matching based on the experimentally determined equivalent thermal conductivity of the simulated lunar soil
9		Specific heat capacity of particles	J/(kg·°C)	228.95 (200–1000)	Experimental measurement
10		Initial temperature of lunar soil	°C	−180	Engineering setting values, with values directly related to the thermal characteristic parameters of the lunar soil, with higher certainty
11	Interaction parameters between lunar soil and drill	Density of the drill	kg/m <sup>3</sup>	7850	Material property
12		Shear modulus of the drill	Pa	8e10	The engineering setting value, for which the value has little influence on the force load simulation, is taken as the material property value in the simulation
13		Poisson's ratio of the drill	-	0.25	Material property
14		Thermal conductivity of the drill	W/(m·K)	44.19 (5–50)	Material property
15		Specific heat capacity of the drill	J/(kg·°C)	544 (400–800)	Material property
16	Heat transfer parameters between lunar soil and drill	Initial temperature of the drill	°C	−115	The engineering settings value, with the values directly related to the thermal characteristics of the drilling tool and indirectly affecting the monthly soil temperature rise
17		Environmental temperature	°C	−240 °C	The engineering settings value
18		Emissivity	-	0.4	Determined by surface conditions with uncertainty
19		Pressure	Pa	$1.01 \times 10^5$ ( $10 \times 10^{-2}$ – $10 \times 10^5$ )	The engineering setting value, with values directly related to thermal parameters, is determined by the experimental environment with high certainty
20		Air convection coefficient	W/(m <sup>2</sup> ·K)	5	The engineering setting value, with a value directly related to the heat transfer effect, is determined by the experimental environment

As shown in Table 3, the lunar soil heat transfer parameters and the machine soil heat transfer parameters have a great influence on the drilling tool and the lunar soil in the sampling area during the sampling process, and their values are uncertain. Among them, the moisture content of the icy lunar soil, the initial temperature of the drilling tool, the initial temperature of the lunar soil, the ambient pressure, and the ambient temperature are determined by the technical conditions. Therefore, the corresponding parameters in this study are the thermal conductivity and the specific heat capacity of the drilling tools and the lunar soil. In addition, the temperature of the drill is significantly warm under the above drilling protocol. The drilling protocol was then optimized to reduce the drilling tool temperature and ensure that ice remained in the lunar soil samples. The optimized drilling speed was determined to be 200 rpm, and the feed rate was 40 mm/min.

### 3.2. Four Factors Combine to Influence the Design of the Simulation Experiments

The main parameters influencing the lunar soil heat transfer parameters and the machine soil heat transfer parameters are the thermal conductivity and specific heat capacity of the lunar soil particles and the drill. In this study, the CCD method was used for the experimental simulation design. The experimental design software was Design-Expert 13. The average lunar soil temperatures in the deep spiral groove at 80 s in the experimental matrix and the simulation results are shown in Tables 4 and 5. The values cover all data from known sources and experimental tests. In addition, we extended these ranges for the four main influencing parameters: the particle thermal conductivity range of 25.75–75.25 W/(m·K), corresponding to a lunar soil thermal conductivity range of 0.26–0.75 W/(m·K), was expanded to a range of 1–100 W/(m·K); the particle specific heat capacity range of 400–800 J/(kg·°C) was expanded to a range of 200–1000 J/(kg·°C); the geometry thermal conductivity range of 16.25–38.75 W/(m·K) was expanded to a range of 5–50 W/(m·K); and the specific heat capacity of the geometry range of 500–700 J/(kg·°C) was expanded to 400–800 J/(kg·°C).

**Table 4.** Parameter impact analysis simulation test matrix and results.

Run Sequence	Thermal Conductivity of Particles (W/(m·K))	Specific Heat Capacity of Particles (J/(kg·°C))	Thermal Conductivity of the Drill (W/(m·K))	Specific Heat Capacity of the Drill (J/(kg·°C))	Drill Bit Temperature (at 80 s; °C)	Lunar Soil Temperature (at 80 s; °C)
1	50.5	600	27.5	600	−123.02	−152.23
2	50.5	1000	27.5	600	−135	−160.11
3	25.75	400	16.25	700	−90.37	−141.4
4	75.25	400	38.75	700	−119.18	−145.66
5	75.25	400	38.75	500	−120.35	−147.24
6	75.25	800	16.25	700	−121.84	−159.09
7	25.75	400	38.75	500	−105.58	−138.93
8	75.25	400	16.25	500	−104.96	−149.72
9	75.25	800	38.75	500	−138.4	−158.94
10	25.75	400	16.25	500	−123.02	−152.23
11	1	600	27.5	600	−51.21	−138.09
12	25.75	800	16.25	500	−113.63	−155.84
13	50.5	600	27.5	800	−121.85	−150.81
14	50.5	600	27.5	600	−92.27	−141.56
15	25.75	400	38.75	700	−105.57	−138.35
16	50.5	600	27.5	600	−123.02	−152.23
17	75.25	800	16.25	500	−124.23	−160.16
18	25.75	800	16.25	700	−108.49	−154.02
19	50.5	200	27.5	600	−83.11	−127.89
20	25.75	800	38.75	500	−125.01	−153
21	75.25	800	38.75	700	−124.41	−153.9
22	50.5	600	27.5	400	−135.95	−156.22

Table 4. Cont.

Run Sequence	Thermal Conductivity of Particles (W/(m·K))	Specific Heat Capacity of Particles (J/(kg·°C))	Thermal Conductivity of the Drill (W/(m·K))	Specific Heat Capacity of the Drill (J/(kg·°C))	Drill Bit Temperature (at 80 s; °C)	Lunar Soil Temperature (at 80 s; °C)
23	25.75	800	38.75	700	−123.25	−152.22
24	50.5	600	5	600	−60.07	−156.68
25	75.25	400	16.25	700	−104.29	−148.51
26	100	600	27.5	600	−128.17	−155.32
27	50.5	600	27.5	600	−123.02	−152.23
28	50.5	600	27.5	600	−123.02	−152.23
29	50.5	600	27.5	600	−123.02	−152.23
30	50.5	600	50	600	−130.09	−150.65

Table 5. Coded and non-encoded values of parameters.

Coded Value	Non Coded Value			
	Thermal Conductivity of Particles (W/(m·K))	Specific Heat Capacity of Particles (J/(kg·°C))	Thermal Conductivity of the Drill (W/(m·K))	Specific Heat Capacity of the Drill (J/(kg·°C))
−a	1	200	5	400
−1	25.75	400	16.25	500
0	50.5	600	27.5	600
+1	75.25	800	38.75	700
+a	100	1000	50	800

### 4. Results Analysis

#### 4.1. The Temperature Rise of the Drilling Simulation

The drill bit temperature and lunar soil temperature are shown in Figure 6. The three groups of coded values −1, 0, and 1 are used as examples:

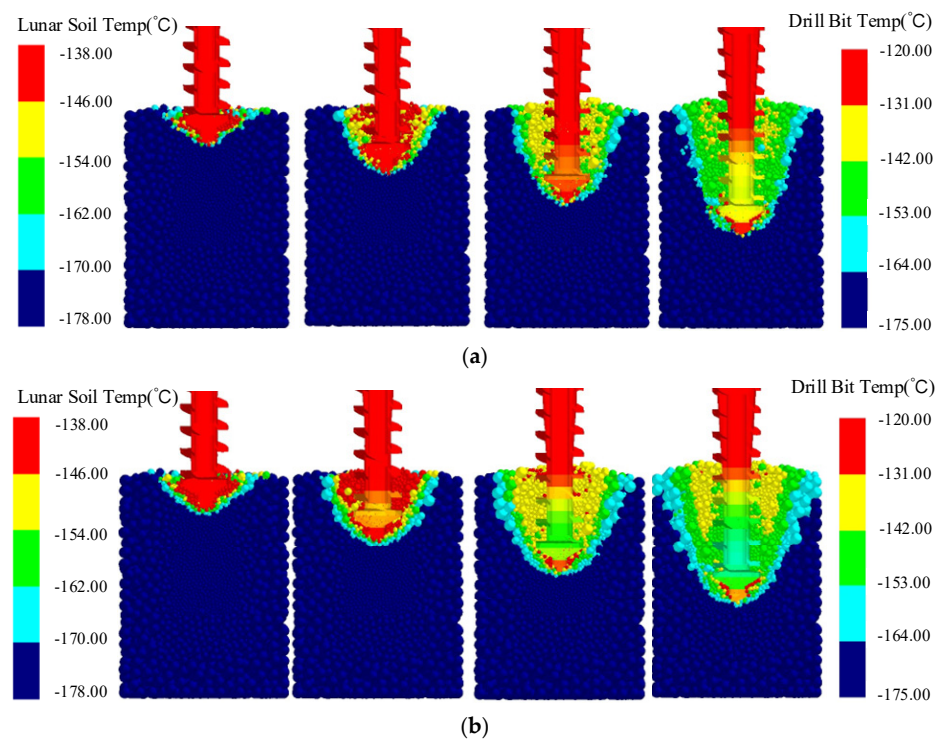
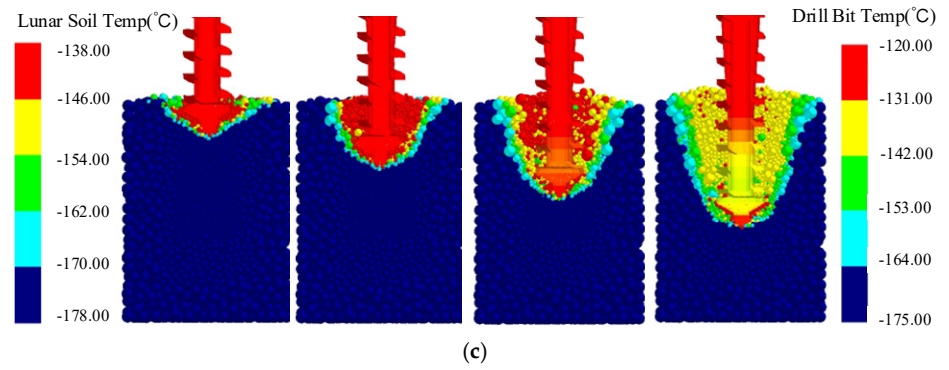
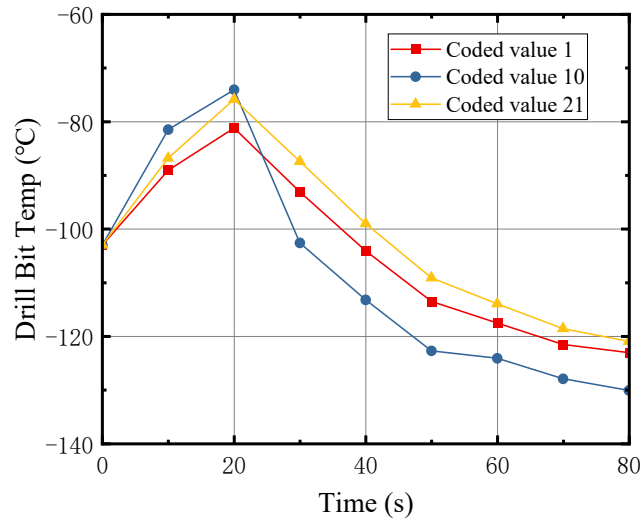


Figure 6. Cont.



**Figure 6.** Drill tool temperature and lunar soil temperature: (a) coded value  $-1$ ; (b) coded value  $0$ ; (c) coded value  $1$ .

The temperature rise curves of the three simulated drill bit scenarios for different heat transfer parameters are shown in Figure 7. The average lunar soil temperature in the deep spiral groove is shown in Figure 8.



**Figure 7.** Temperature rise curve of the drill bit.

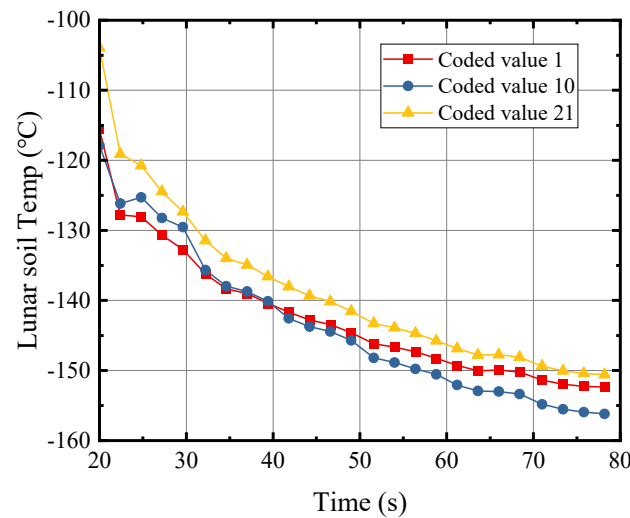


**Figure 8.** Average lunar soil temperature in the deep spiral groove.

The simulation results show that when the drilling thermal parameters changed, the area affected by the drilling temperature rise also changed. Meanwhile, the temperature of the lunar soil particles near the drilling tool varied greatly. The initial temperature of the drilling tool was higher than the initial temperature of the lunar soil, but the low temperature of the icy lunar soil cooled the drilling tool. As a point heat source, the drilling tool temperature showed a tendency to increase and then decrease under the combined effect of the heat generated by cutting and the cooling by the low-temperature lunar soil. The average temperature of the icy lunar soil in the deep spiral groove gradually decreased with increasing drilling depth. The temperature trend was the same as that of the microelement at the rear end of the drill.

The results of the significance analysis of the effect of thermal parameters showed that  $K_p$ ,  $C_p$ , and  $K_g$  had significant effects on the temperature of the front end of the drill bit.  $K_p$ ,  $C_p$ ,  $K_g$ , and  $C_g$  had significant effects on the average lunar soil temperature in the deep spiral groove. A quadratic regression equation was used to fit the experimental results. The relationship between the drill bit temperature and the average icy lunar soil temperature in the deep spiral groove and the main influencing parameters were obtained as follows:

$$Drill\ Bit\ Temp = +15.23046 - 1.52518K_p - 0.0525020C_p - 3.223210K_g + 0.010784K_p^2 + 0.041550K_g^2 \tag{3}$$

$$Lunar\ soil\ Temp = -104.75921 - 0.447922K_p - 0.101152C_p + 0.117774K_g + 0.006708C_g + 0.000146K_pC_p + 0.002156K_p^2 + 0.000050C_p^2 \tag{4}$$

where  $K_p$  is the thermal conductivity of lunar soil particles;  $C_p$  is the specific heat capacity of lunar soil particles;  $K_g$  is the thermal conductivity of the drill;  $C_g$  is the specific heat capacity of the drill. Lunar soil temp is the average temperature of the lunar soil in the deep spiral trough; drill bit temp is the temperature of the drill bit.

#### 4.2. Single-Factor Impact Analysis

A single-factor influence analysis was performed, and the trend of the influence of the four factors on the average icy lunar soil temperature in the deep spiral groove is shown in Figure 9. The dashed line in the Figure 9 shows the 95% confidence interval. The temperature data are for an 80 s simulation.

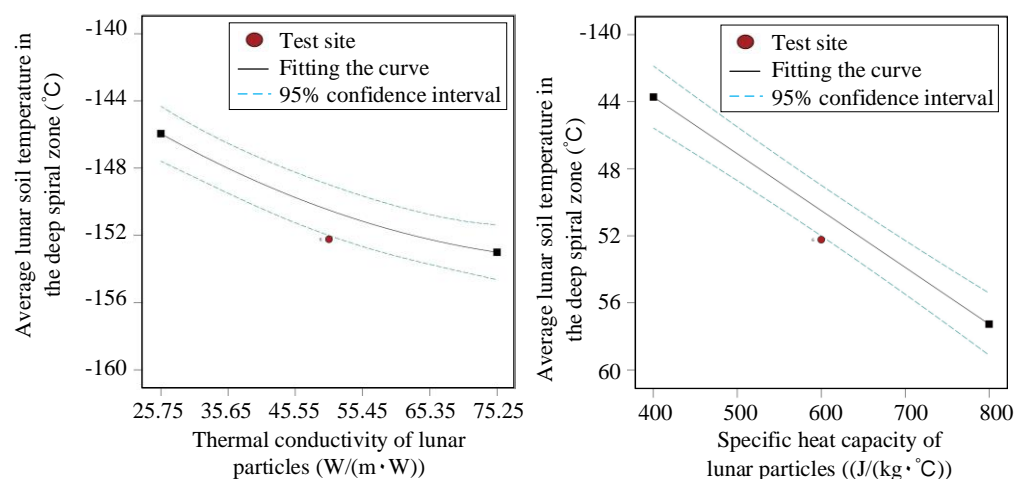
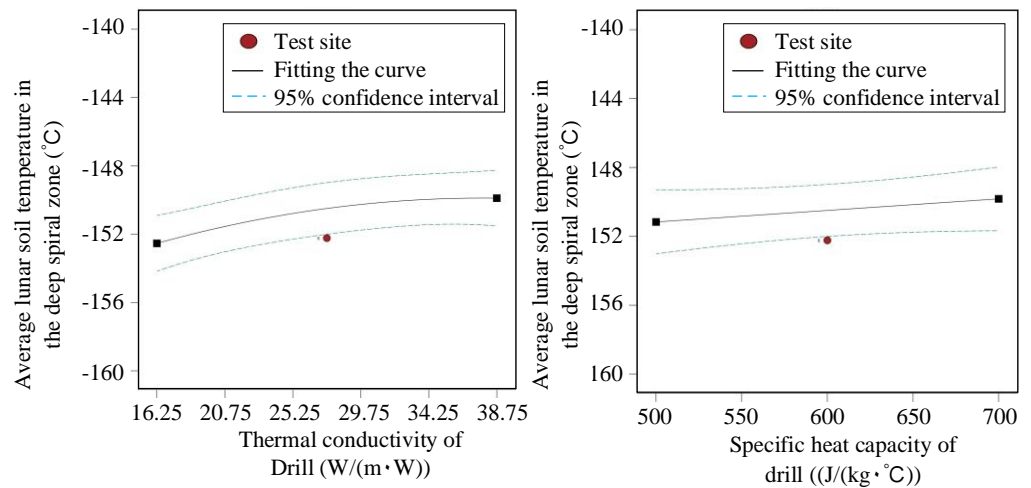


Figure 9. Cont.



**Figure 9.** Trends in the influence of four factors on the average lunar soil temperature in the deep spiral groove.

Within the parameters of the technical documentation, the average temperature of the icy lunar soil ranged from  $-143$  to  $-158$  °C. The thermal conductivity and specific heat capacity of the lunar soil particles had significant effects on the average temperature of the icy lunar soil in the deep spiral groove, and their values were negatively correlated with the temperature of the lunar soil. The thermal conductivity and heat capacity of the drill had a weak positive correlation effect with the average temperature of the lunar soil in the deep spiral groove.

The trend of the influence of  $K_p$ ,  $C_p$ , and  $K_g$  factors on the drill bit temperature is shown in Figure 10.

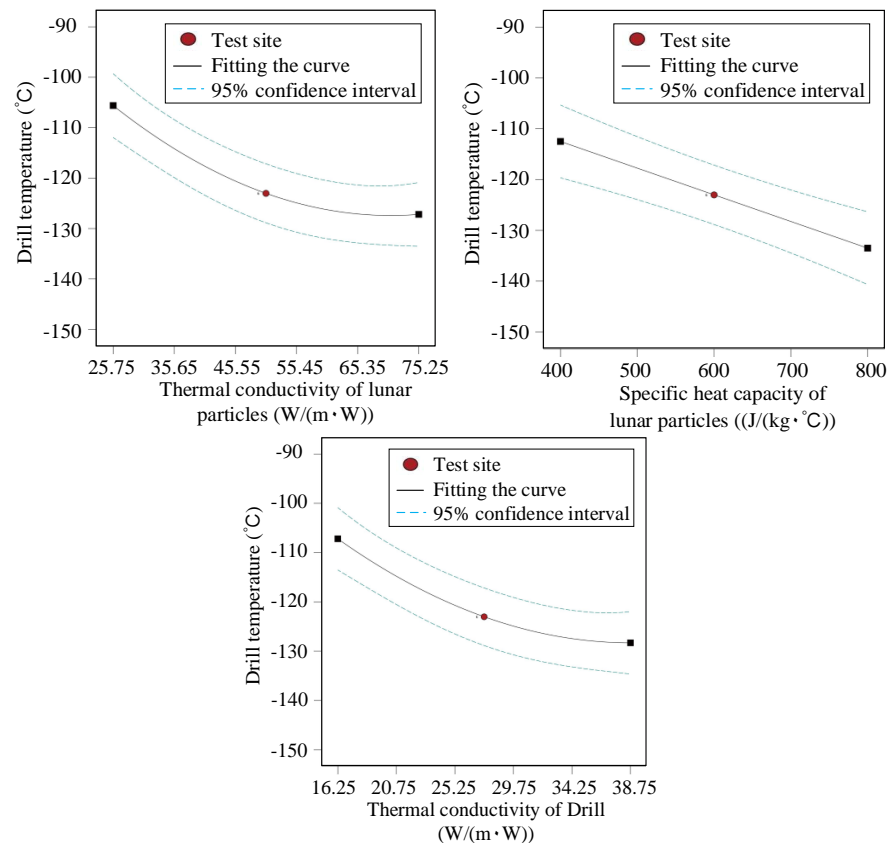


**Figure 10.** Trend of the effect of three factors on the temperature of the front end of the drill bit.

Within the parameters of the engineering documentation, the drill bit temperature variation interval ranged from  $-105$  to  $-132$  °C. The thermal conductivity of the lunar soil particles, the specific heat capacity of the icy lunar soil, and the thermal conductivity of the drill had a significant negative correlation with the drill bit temperature.

### 4.3. Two-Factor Impact Analysis

From Equations (3) and (4), the significant influencing factors of the average monthly soil temperature in the deep spiral groove included  $K_p$ ,  $C_p$ ,  $K_g$ , and  $C_g$ , while the significant influencing factors of the drill bit temperature included  $K_p$ ,  $C_p$ , and  $K_g$ . In the two-factor analysis, the significant factors influencing the average lunar soil temperature in the deep spiral groove could be divided into six groups, and the trend is shown in Figure 11. The significant factors influencing the drill bit temperature could be divided into three groups, and the trend is shown in Figure 12.

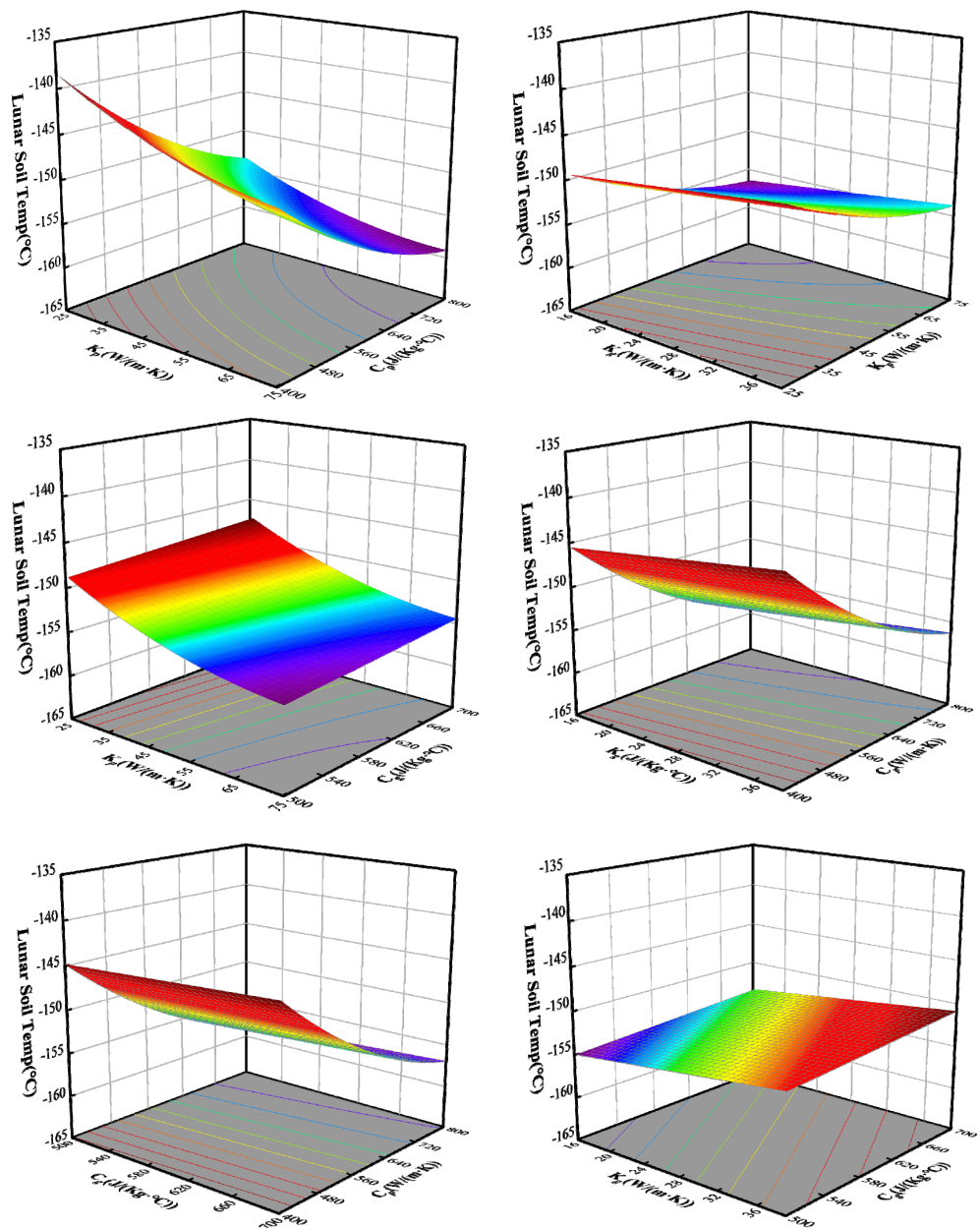


**Figure 11.** Trend of the influence of two factors on the mean temperature of the lunar soil within the deep spiral of the lunar soil.

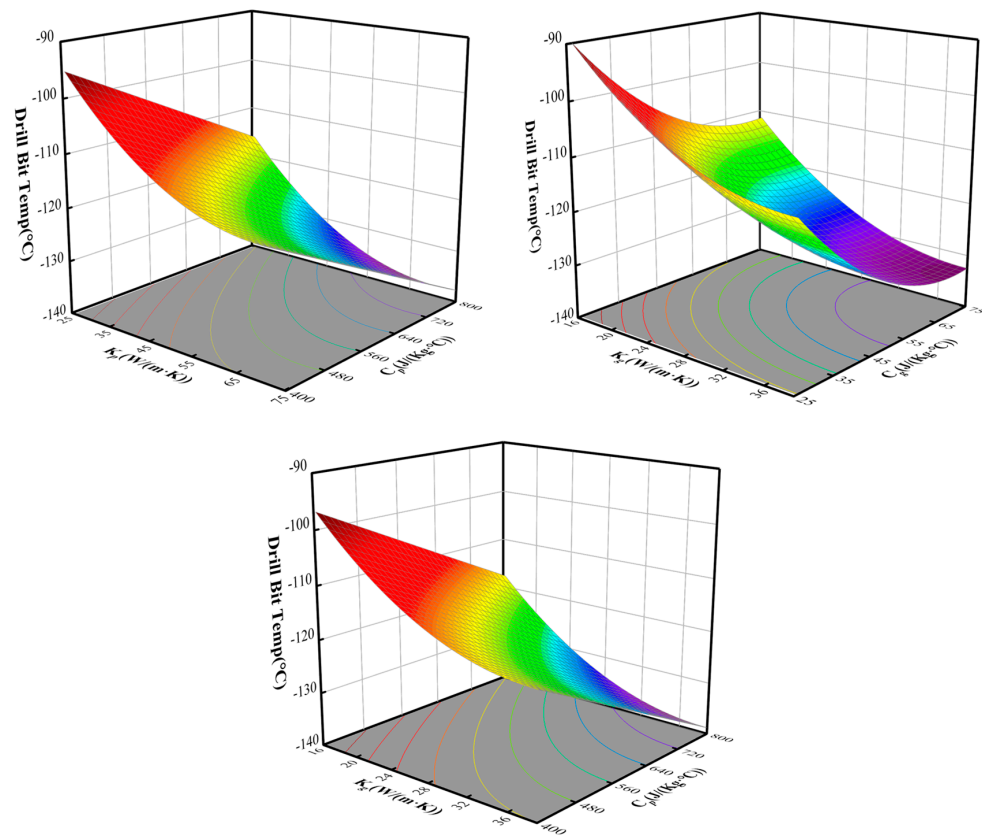


**Figure 12.** Trend of the influence of two factors on drill bit temperature.

In the analysis of the two-factor effect on the average temperature of the icy lunar soil in the deep spiral groove, the combined thermal conductivity and specific heat capacity of the lunar soil particles had the largest effect, while the conductivity and specific heat capacity of the drill had the smallest effect. Furthermore, the icy lunar soil did not undergo a solid–gas phase transition in this temperature range.

The analysis of the effect of two factors on the temperature of the drill bit, the thermal conductivity and specific heat capacity of the particles, and the thermal conductivity of the drill had a significant effect on the drill bit temperature. The latter had the most significant effect. In addition, in the temperature interval, the spiral groove structure sampling method was feasible under the engineering setting drilling protocols.

## 5. Conclusions

In this paper, lunar soil was collected through a spiral groove structure. The effect of the thermal parameters of the lunar soil particles and the drill on the temperature of the icy lunar soil in the drilling groove was analyzed by DEM. The temperature range of the lunar soil samples with different thermal parameters was obtained. The results showed that for a drilling protocol with a rotation speed of 200 rpm and a feed rate of 40 mm/min, the drill temperature ranged from  $-51.21$  to  $-135.00$  °C, and the average temperature of the icy lunar soil in the deep spiral trough was between  $-127.89$  and  $-160.16$  °C. The peak temperature of the lunar soil samples was always below  $-70$  °C. The sample did not undergo a phase change from solid to gas. This demonstrated the feasibility of the spiral groove structure for sampling. The study provides data support for drilling tools to collect lunar soil, obtains the temperature ranges of lunar soil particles and drill bits during drilling in a low-temperature vacuum environment through numerical simulation, and analyzes the trends of the four main factors affecting the temperatures of the lunar soil and drill bits. Based on the simulation results, appropriate drilling tool parameters are selected

so as to minimize the solid–gas phase transition of water ice in the lunar soil as much as possible during the mining process.

The main parameters in the thermal impact analysis included the thermal conductivity and specific heat capacity of the lunar soil particles and the drill. The effects of the four factors on the temperature of the lunar soil and the temperature of the drill in the deep spiral groove were as follows: (1) The thermal conductivity and specific heat capacity parameters of the lunar soil particles had a more significant effect on the system temperature variation. The value was also negatively correlated with the drill temperature and the average icy lunar soil temperature in the deep spiral groove. (2) The thermal conductivity and specific heat capacity parameters of the drill had slightly weaker effects on the system temperature variation. The main effect was reflected in a certain negative correlation between the thermal conductivity of the drill and the drill bit temperature. In addition, there was a relatively weak positive correlation between the thermal conductivity and specific heat capacity of the drill and the average lunar soil temperature in the deep spiral groove. To control the temperature of lunar soil samples, sampling can be accomplished by selecting drill materials with lower thermal conductivities and specific heat capacities.

**Author Contributions:** Conceptualization, D.Z. and W.Z.; Methodology, D.Z.; Software, T.P. and H.W.; Validation, T.P., W.Z. and J.C.; Formal analysis, T.P. and H.W.; Investigation, T.P.; Resources, W.Z.; Data curation, T.P., W.Z. and J.C.; Writing—original draft, D.Z., T.P. and H.W.; Writing—review & editing, D.Z., W.Z. and J.C.; Visualization, T.P.; Supervision, W.Z.; Project administration, D.Z. and W.Z.; Funding acquisition, D.Z. and W.Z. All authors have read and agreed to the published version of the manuscript.

**Funding:** This project is financially supported by fundamental research funds for the National Natural Science Foundation of China [No. 51805488, No. 52005136] and the Science and Technology Program of Guangzhou, China. [No. 202102020320].

**Data Availability Statement:** The data that support the findings of this study are available from the corresponding authors upon reasonable request.

**Conflicts of Interest:** The authors declare no conflict of interest. The funders had no role in the design of the study; in the collection, analyses, or interpretation of data; in the writing of the manuscript; or in the decision to publish the results.

## References

1. Anand, M. Lunar Water: A Brief Review. *Earth Moon Planets* **2010**, *107*, 65–73. [[CrossRef](#)]
2. Du, Y.; Sheng, L.; Zhang, H.; Ma, J.L.; Zhang, H.; Li, F.; Wu, K. Analysis of the occurrence mode of water ice on the moon and the prospect of in-situ lunar exploration. *Spacecr. Environ. Eng.* **2019**, *36*, 8.
3. Wu, W.; Yu, D.; Wang, C.; Liu, J.; Tang, Y.; Zhang, H.; Zou, Y.; Ma, J.; Zhou, G.; Zhang, Z.; et al. Research on the Main Scientific and Technological Issues on Lunar Polar Exploration. *J. Deep Space Explor.* **2020**, *7*, 223–231+240.
4. Vasavada, R.; Paige, D.A.; Wood, S.E. Near-surface temperatures on Mercury and the Moon and the stability of polar ice deposits. *Icarus* **1999**, *141*, 179–193. [[CrossRef](#)]
5. Nozette, S.; Spudis, P.D.; Robinson, M.S.; Bussey, D.B.J.; Lichtenberg, C.; Bonner, R. Integration of Lunar polar remote-sensing data sets: Evidence for ice at the Lunar south pole. *J. Geophys. Res. Planets* **2001**, *106*, 23253–23266. [[CrossRef](#)]
6. Thomson, B.J.; Bussey, D.B.J.; Neish, C.D.; Cahill, J.T.S.; Heggy, E.; Kirk, R.L.; Patterson, G.W.; Raney, R.K.; Spudis, P.D.; Thompson, T.W.; et al. An upper limit for ice in Shackleton crater as revealed by LRO Mini-RF orbital radar. *Geophys. Res. Lett.* **2012**, *39*, L14201. [[CrossRef](#)]
7. Honniball, C.I.; Lucey, P.G.; Li, S.; Shenoy, S.; Orlando, T.M.; Hibbitts, C.A.; Hurley, D.M.; Farrell, W.M. Molecular water on the illuminated lunar surface: Detection of the 6  $\mu$ m H-O-H fundamental with the SOFIA airborne observatory. In Proceedings of the 51st Lunar and Planetary Science Conference, The Woodlands, TX, USA, 16–20 March 2020.
8. Colaprete, A.; Schultz, P.; Heldmann, J.; Wooden, D.; Shirley, M.; Ennico, K.; Hermalyn, B.; Marshall, W.; Ricco, A.; Elphic, R.C.; et al. Detection of water in the LCROSS ejecta plume. *Science* **2010**, *330*, 463–468. [[CrossRef](#)] [[PubMed](#)]
9. Haruyama, J.; Ohtake, M.; Matsunaga, T.; Morota, T.; Honda, C.; Yokota, Y.; Pieters, C.M.; Hara, S.; Hioki, K.; Saiki, K.; et al. Lack of exposed ice inside lunar south pole Shackleton Crater. *Science* **2008**, *322*, 938–939. [[CrossRef](#)] [[PubMed](#)]
10. Liu, D.; Zhang, H.; Yang, S.; Yin, C.; Zhang, J.; Sun, Q.; Lai, X. Research of Drilling and Sampling Technique for Lunar Polar Region Exploration. *J. Deep Space Explor.* **2020**, *7*, 278–289. [[CrossRef](#)]
11. Zhao, D.; Tang, D.; Hou, X.; Jiang, S.; Deng, Z. Soil chip convey of lunar subsurface auger drill. *Adv. Space Res.* **2016**, *57*, 2196–2203. [[CrossRef](#)]

12. Cui, J.; Hou, X.; Wen, G.; Liang, Z. DEM thermal simulation of bit and object in drilling of lunar soil simulant. *Adv. Space Res.* **2018**, *62*, 967–975. [[CrossRef](#)]
13. Vargas, W.L.; McCarthy, J.J. Thermal expansion effects and heat conduction in granular materials. *Phys. Rev. E* **2007**, *76*, 041301. [[CrossRef](#)]
14. Cui, J. Research on Mechanics-Thermotics Characteristic of Drill-Lunar Regolith Interaction and Prediction of The Temperature Field. Ph.D. Thesis, Harbin Institute of Technology, Harbin, China, 2016.
15. Cui, J. Research on Filling Model and Characteristic of Lunar Soil Simulant. Master's Thesis, Harbin Institute of Technology, Harbin, China, 2011.
16. Zhao, D.; Hou, X.; Tang, D.; Yuan, J.; Jiang, S.; Deng, Z. DEM parameter matching of high-dense lunar soil simulant. In Proceedings of the IEEE International Conference on Information & Automation, Lijiang, China, 8–10 August 2015; IEEE: Piscataway, NJ, USA, 2015.
17. Deng, Z.; Cui, J.; Hou, X.; Jiang, S. Calibration of Discrete Element Heat Transfer Parameters by Central Composite Design. *Chin. J. Mech. Eng.* **2017**, *30*, 419–427. [[CrossRef](#)]
18. Li, S.; Lucey, P.G.; Milliken, R.E.; Hayne, P.O.; Fisher, E.; Williams, J.-P.; Hurley, D.M.; Elphic, R.C. Direct evidence of surface exposed water ice in the lunar polar regions. *Proc. Natl. Acad. Sci. USA* **2018**, *115*, 8907–8912. [[CrossRef](#)] [[PubMed](#)]
19. Mitchell, J.K.; Houston, W.N.; Carrier, W.D., III; Costes, N.C. Apollo soil mechanics experiment S-200. *Arch. Dermatol. Syphilol.* **1974**, *53*, 73.
20. Carrier, W.D., III; Olhoeft, G.R.; Mendell, W. Physical Properties of the Lunar Surface. In *Lunar Sourcebook, A User's Guide to the Moon*; Cambridge University Press: Cambridge, UK, 1991.

**Disclaimer/Publisher's Note:** The statements, opinions and data contained in all publications are solely those of the individual author(s) and contributor(s) and not of MDPI and/or the editor(s). MDPI and/or the editor(s) disclaim responsibility for any injury to people or property resulting from any ideas, methods, instructions or products referred to in the content.